Int. J. Electrochem. Sci., 14 **(2019)** 3651 – 3662, doi: 10.201964/2019.04.29

International Journal of
ELECTROCHEMICAL
SCIENCE
www.electrochemsci.org

Effect of Aging Treatment on Corrosion Resistance of S32750 Super Duplex Stainless Steel in Simulated Seawater at Low Temperature

Lan Jin, Ping Liang[*]*, Yanhua Shi, Yier Guo, Yan Zhao, Fei Li, Guanyu Hou*

School of Mechanical Engineering, Liaoning Shihua University, Fushun 113001, China
[*]E-mail: liangping770101@163.com

Received: 30 November 2018 / *Accepted:* 28 January 2019 / *Published:* 10 March 2019

Electrochemical corrosion behaviors of S32750 super duplex stainless steel (SDSS) with different temperature aging treatment range from 650 ℃ to 850 ℃ in the simulated seawater were investigated by means of potentiodynamic polarization curves, electrochemical impedance spectroscopy (EIS) and Mott-Schottky curves measurements. Microstructures of samples at different aging temperature were observed, and the phases presented in the heat-treated SDSS samples were also characterized by X-ray diffraction (XRD). In addition, the corrosion morphology after polarization was observed by optical microscope (OM). The results showed that the σ phase was not precipitated at 650 ℃, while it was found in the temperature range from 750 ℃ to 850 ℃. Furthermore, the amount of σ phase was the most when aging at 850℃, and the passive film became uneven and less dense with increasing aging temperature. The corrosion resistance of S32750 SDSS declined with the aging temperature was mainly ascribed to that the precipitation of σ phase reduced the stability and thickness of the passive film, and the corrosion reaction was accelerated.

Keywords: Aging Temperature, σ Phase, S32750 Super Duplex Stainless Steel, Simulated Seawater

1. INTRODUCTION

Duplex stainless steel (DSS) possessed a two-phase microstructures of austenite and ferrite, the content of dual phase structure was almost the same, so DSS had an attractive combination of superior mechanical strength and higher corrosion resistance in various aggressive environments, as compared to the conventional austenitic stainless steel. The super duplex stainless steel (SDSS), called the third-generation duplex stainless steel, had a ultra-low carbon, high chromium, high nitrogen and other components, which greatly improved the duplex stainless steel comprehensive properties, such as toughness, weld ability and corrosion resistance. Therefore, it was widely used in many engineering applications such as petrochemical, natural gas, shipbuilding, marine, military, transport and many other

fields [1-4].

S32750 SDSS, a typical third-generation duplex stainless steel, displayed excellent properties of austenitic stainless steel and ferritic stainless steel. However, due to its high degree of alloying, it was easy to form carbide ($M_{23}C_6$), nitride (Cr_2N), σ phase, χ phase and other intermetallic compounds in the solidification stage or welding, and these precipitates may have adverse effects on material structure, corrosion properties,mechanical properties, and so on. Zuo reported that S32750 SDSS began to precipitate σ phase after 2 minutes of heat treatment, and the toughness of the material decreased due to the presence of σ phase [5]. Bhattacharya and Singh found that the S32205 SDSS annealed at 800 ℃, sigma and chi precipitates were produced in the SDSS sample, while the samples aged at 800 ℃did not show susceptibility to SCC. But the sample annealed at 1150 ℃ and aged at 475 ℃ both displayed severe intergranular SCC [6].

The ocean was a vast treasure trove of resources which was abundant in mineral resources, biol -ogicalresources, water resources, etc. So, it became a priority area for the economic and human development, science and technology development. However, the seawater as an extremely complex corrosive media had severe corrosion hazards to ships and marine engineering equipment working in the marine environment [7-10]. Therefore, it was of great significance to improve the corrosion resistance and ensure the service life and safety of the equipments. S32750 SDSS had an excellent comprehensive performances, which was possible to replace ordinary duplex stainless steel and other materials and became an ideal marine engineering material. However, the precipitation phases inside the S32750 SDSS during aging treatment may cause the corrosion resistance of S32750 SDSS to decrease in seawater. This paper mainly investigates the microstructure changes of S32750 SDSS at different aging temperatures and the corrosion behavior of S32750 SDSS in seawater at low temperature environment, and the ultimate aim was to provide some references for the engineering applications of S32750 SDSS in seawater environment.

2. EXPERIMENTAL

2.1 Material and test preparation

The SDSS S32750 plates were used as the investigated material in this study, and the element composition of which is listed in Table 1.

The corrosion medium in the experiments was 3.5% NaCl solution used to simulate the seawater environment. During the measurements, the solution temperature was kept at 5±0.1 ℃ using a HH-6 type water bath.

Prior to the experiments, the S32750 SDSS was cut into a sheet sample, and the processed samples were aged at 650 ℃, 750 ℃ and 850 ℃for 20 minutes, respectively, and then cooled in air. The samples were sealed after the completed cooling by epoxy resin with a working area of 1 cm^2 followed by grinding sequentially with SiC papers from 180 to 2000 grit, and washed with deionized water and rinsed by anhydrous ethanol, and then dried in a desiccator [11].

Table 1. Chemical composition of S32750 SDSS in this study (wt %)

steel	C	Si	Mn	S	P	Cr	Ni	Mo	N	Fe
S32750 SDSS	0.021	0.49	0.75	0.0001	0.025	25.02	6.28	3.54	0.252	Bal.

2.2 Electrochemical measurements

The prepared sample were polished and etched for 1 to 3 minutes in 30 g KOH + 30g $K_3Fe(CN)_6$ + 100 mL deionized water solution at 85 ℃. After the sample was etched, it was washed and dried, and the microstructures were observed using a Leica QM500 metallographic microscope and scanning electron microscope (SEM), and the contents of elements were tested with Energy Dispersion Spectrum (EDS), and the phase compositions of samples were analyzed by means of X-7000 X-ray diffractometer (XRD).

Electrochemical measurements were carried out with a traditional three-electrode cell systems provided by the PARSTAT 2273 electrochemical workstation. The S32750 SDSS samples with aging treatment were used as the working electrode (WE), Pt sheet served as the counter electrode (CE), saturated calomel electrode (SCE) as the reference electrode. All potentials in the work were relative to SCE [11].

The electrochemical polarization curves of S32750 SDSS samples aged at different temperature in seawater at 5 ℃ were performed.

Electrochemical impedance spectroscopy (EIS) were carried out using AC signals with an amplitude of 10 mV in the frequency range from 100 kHz to 100 mHz. The measured EIS data was fitted using Zview 3.20 software.

The specimens were immersed in the solution for 1 hour in order to reach a nearly steady-state open-circuit potential values (OCP), and then the potentiodynamic polarization curves were obtained starting from a potential -0.3 to 1.3 V at a scan rate of 1.0 $mV \cdot s^{-1}$. The corrosion behavior of S32750 SDSS was evaluated accroding to the pitting potential E_b, corrosion current density i_{corr} and corrosion potential E_{corr} established from polarization curves.

The Mott-Schottky curves were obtained by measuring the capacitance of the passive film formed on the S32750 SDSS specimens. The potential was scanned in the range from -0.4 to 0.6 V. An AC excitation 10 mVsignal amplitude in the frequency of 1000 Hz was adopted to the system [11].

3. RESULTS & DISCUSSION

3.1 Micromorphology

The microstructures of SDSS S32750 at different aging temperature are shown in Figure 1. It could be observed from the optical micrographs of the microstructures of SDSS S32750 at solid solution condition and the aging temperature consisted of white banded austenite phase and dark gray banded ferrite phase. No precipitation phase was found in the sample aged at 650 ℃. A small amount of black

precipitates appeared on the ferrite and austenite grain boundaries when the aging temperature increased to 750 ℃, and the volume content of precipitated phase increased with the aging temperature arsing to 850 ℃, and the grain boundaries of ferrite phase were coarsened, and the content of ferrite phase was relatively reduced.

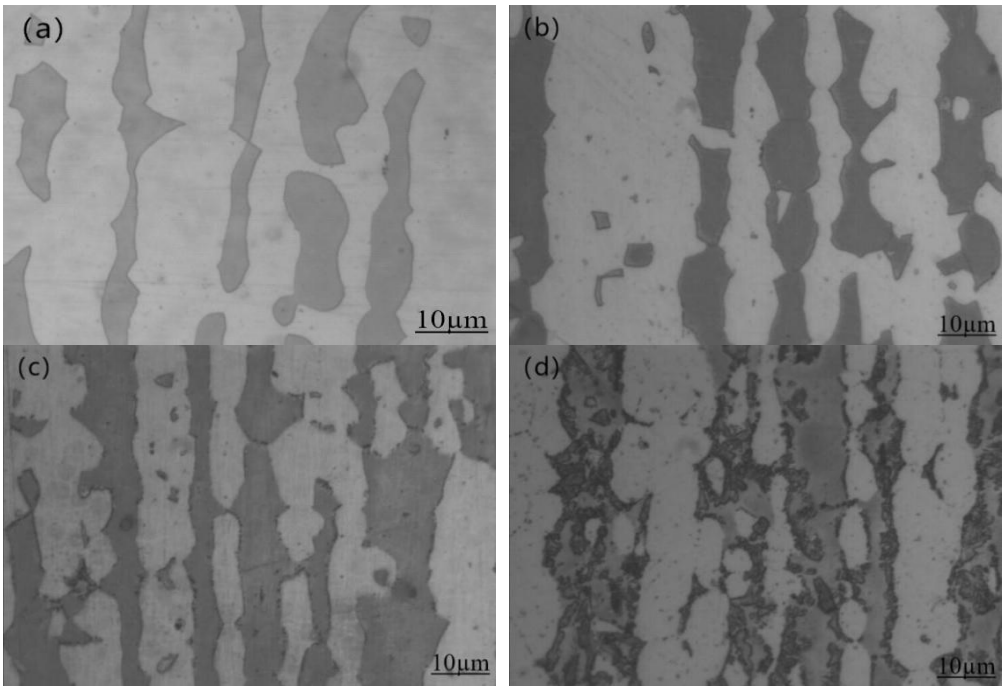

Figure 1. Microstructure images of S32750 SDSS at different aging temperatures (a) solid solution condition, (b)650 ℃, (c)750 ℃, (d) 850 ℃

3.2 Precipitates analysis

The XRD patterns of the S32750 SDSS at different aging temperatures are list in Figure 2. It displayed that no precipitates of σ phase was detected in the XRD pattern at the solid solution condition and 650 ℃, and only the γ phase and the α phase existed. When the aging temperature increased to 750 ℃, the σ phase diffraction peak appeared in the XRD pattern, indicating that there was σ phase precipitation. As the aging temperature was further up to 850 ℃, the σ precipitation phase increased, which leaded to the decrease of α phase. Therefore, the α phase gradually decreased and the σ phase and γ phase increased as the aging temperature from 650 ℃ up to 850 ℃.

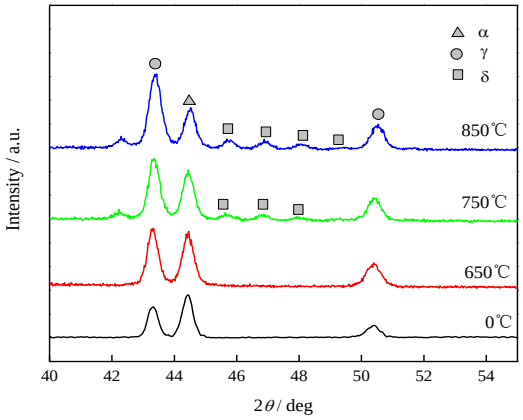

Figure 2. XRD spectra of S32750 SDSS at different aging temperatures

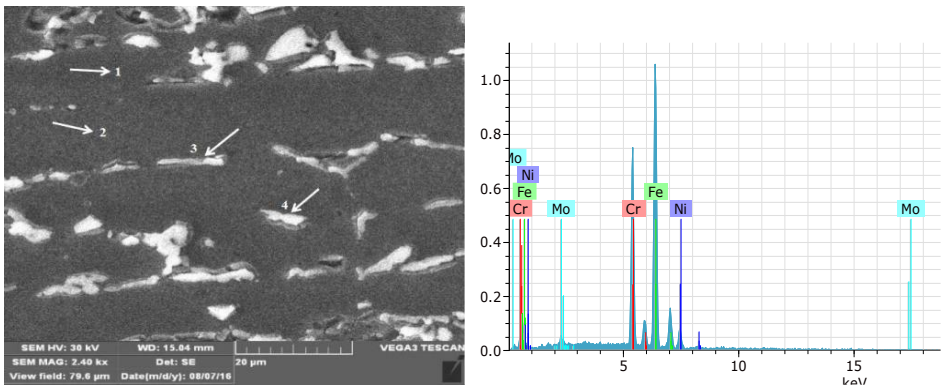

Figure 3. SEM image of S32750 SDSS at aging temperature of 850℃

Table 2. Chemical compositions at each point in Figure 3 (wt %)

Test positions	Phase	Cr	Ni	Mo
Zone 1	γ	25.16	6.89	2.17
Zone 2	α	25.78	6.02	4.62
Zone 3	σ	27.84	4.21	5.63
Zone 4	γ_2	25.42	7.63	1.90

From the above analysis, it may be seen that there were precipitated phases at aging temperatures of 750 ℃ and 850 ℃. Figure 3 demonstrates SEM image of the S32750 SDSS aging at 850 ℃ for 20 minutes. Test and analysis of Cr, Mo and Ni contents at 1, 2, 3 and 4 positions in Figure 3 by EDS technique, the results are presented in Table 2. At point 1 area, the content of Cr and Mo was lower, and the content of Ni was higher, which was determined as austenite γ phase. At point 2 area, the content of Cr and Mo was higher, and the content of Ni was lower, which was determined as ferrite α phase. At

point 3 area, a white banded, the content of Cr and Mo was higher than the average content of both Cr and Mo in the material, and Ni was significantly reduced, combined with XRD analysis, it could be inferred that the precipitation was mainly σ phase. At the point 4 area, the Cr and Mo content decreased, Ni increased significantly, and it was higher than the average Ni content of the material, which could be determined as the secondary austenite phase (γ_2) [12-15].

3.3 Effect of aging temperature on potentiodynamic polarization

The polarization curves provided some important information concerning the electrochemical behavior of S32750 SDSS. Figure 4 exhibites the potentiodynamic polarization curves of S32750 SDSS with the solid solution condition and different aging temperatures in simulated seawater at 5 ℃. It could be seen that the all samples showed an obvious passivation zone, meaning that S32750 SDSS could display a good corrosion resistance because of passive films formed on S32750 SDSS in the test conditions.

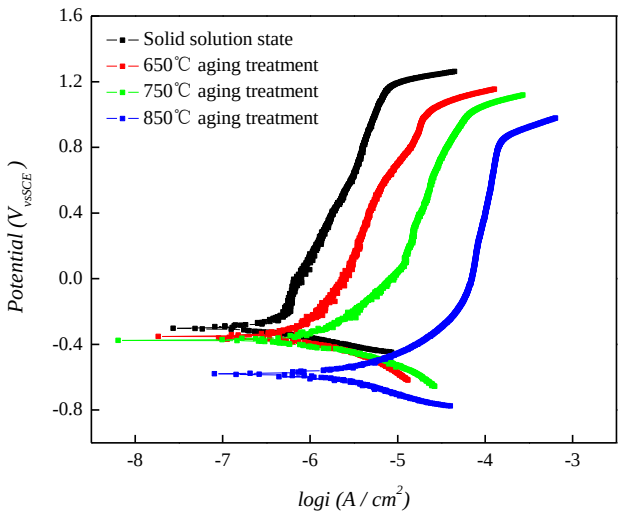

Figure 4. Polarization curves of SDSS S32750 in simulated seawater at different aging temperatures

The fitted results of polarization curves are demonstrated in Table 3. It seemed that the investigated sample with solid solution condition had the best corrosion resistance, due to the most noble E_{corr} and E_b values, the lowest i_{corr} and i_p values. With increasing aging temperature from 650 ℃ to 850 ℃, the polarization curves gradually moved to the right and in the negative direction, and during the polarization process, as the potential increased, the current density also increased accordingly, which indicating that the aging treatment reduced the corrosion resistance of S32750 SDSS. Moreover, the higher the aging temperature, the worse the corrosion resistance. It was because that Cl^- in the solution took a great influence on the pitting of the S32750 SDSS, when the potential raised to a certain value, the corrosion rate of the passive films was greater than that of the repair speed for the films, resulting in the failure of the passive film to be repaired in time. When the potential reached the pitting potential, a large number of pitting pits appeared on the surface of the material, and the corrosion resistance of S32750 SDSS was weakened. When the aging temperature increased from 650 ℃ to 850 ℃, the value

of E_{corr} and E_b decreased and i_{corr} increased gradually. When the aging temperature was to 850 ℃, the values of E_{corr} and i_{corr} were 2.5 times and 5 times those of under solid solution condition, respectively. In addition, Tafel slopes (β_a) as well as the anode region and the value of i_p after aging treatment also increased as increasing aging temperature. The dissolution rate of passive films on S32750 SDSS in simulated seawater increased slowly, implying that the aging temperature reduced the corrosion resistance of S32750 SDSS.

Table 3. Fitting results of potentiodynamic polarization curves of S32750 SDSS at different aging temperatures in simulated seawater at a scan rate of 1.0 $mV \cdot s^{-1}$

Aging Temperatures	$E_{corr}(mV_{SCE})$	$E_b(V_{SCE})$	$i_{corr}(\mu A \cdot cm^{-2})$	$i_p(\mu A \cdot cm^{-2})$	$\beta_a(mV/decade)$
solid solution condition	-257	1.25	12.9	10.1	0.219
650℃	-320	1.12	16.4	15.6	0.263
750℃	-407	1.03	25.1	22.3	0.317
850℃	-634	0.98	56.3	39.8	0.426

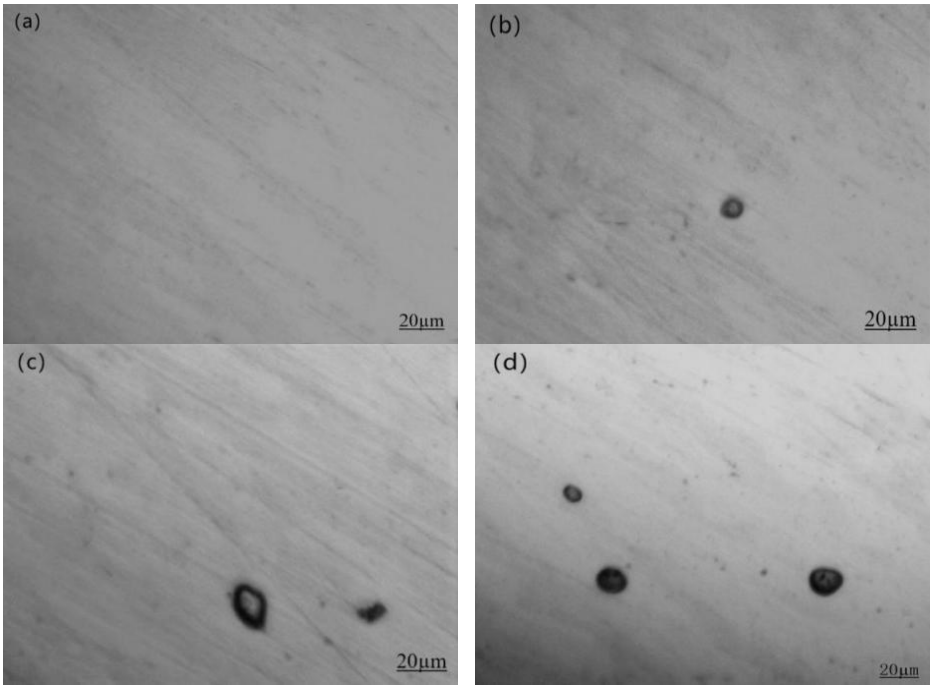

Figure 5. Corrosion morphology of SDSS S32750 at different aging temperatures after potentiodynamic polarization tests (a) solid solution condition, (b) 650 ℃, (c) 750 ℃, (d) 850 ℃

Observations of the corrosion morphology of the investigated samples after polarization at different aging temperatures. The surface morphologies of the samples revealed that there was no

significant corrosion on the surface of the sample under solid solution condition (Figure 5a), and with the increase of aging temperature, pitting pits appeared on the surface, and the numbers and pits diameters gradually increased (Figure 5b, c, d), meaning that the corrosion became more serious.

3.4 Electrochemical Impedance Measurement

Figure 6 gives the Nyquist curves for S32750 SDSS with different aging temperature in simulated seawater. It could be found from Figure 6(a) that the Nyquist curves of the samples under different conditions were capacitive semicircle loops, indicating that the surface of the sample could form a complete passive film [16]. The aging temperature increased from 650 ℃ to 850 ℃, the semicircle diameter of capacitive loops decreased gradually, meaning that the polarization resistance in the electrochemical reaction and the corrosion resistance of S32750 SDSS decreased. As can be seen from the Bode plots of Figure 6(b), it expressed two time constants [17]. In the low-frequency region of the bode plots, the impedance modulus represented the polarization resistance of the electrode, and the high-frequency region impedance modulus value reflected the solution resistance [18]. As the aging temperature increased, the polarization resistance and solution resistance of the S32750 SDSS decreased, the stability of the passive film worse, and the corrosion rate increased, which was consistent with the results obtained by the polarization curves.

An equivalent electrical circuit provided in Figure 7 is used to fit the EIS data [19], and the fitted results are presented in Figure 8. In this equivalent electrical circuit, R_s is the electrolyte solution resistance, R_{film} is the resistance of passive film, CPE_{film} is the subsequent passive layer, R_{ct} is the charge transfer resistance, CPE_{dl} represents the capacitance of the passive film including the defects. The non-ideal electric behavior was taken into account by introducing a constant phase element (CPE) . The values of R_{ct} and R_{film} were the largest for the samples under solid solution condition, while both of them reduced with increasing aging temperature, according to Fig.8.

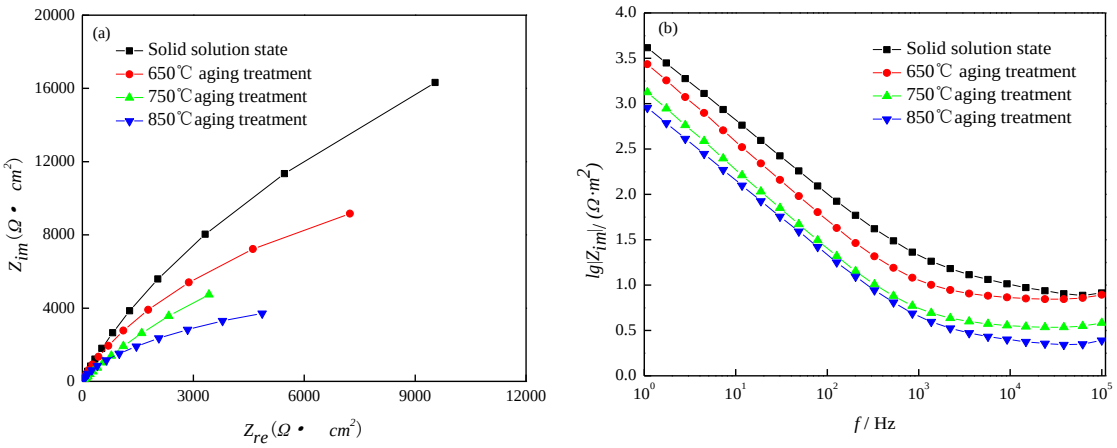

Figure 6. EIS of S32750 SDSS for different aging temperatures in 3.5 % NaCl solution (a) Nyquist curves, (b) bode phase value against frequency

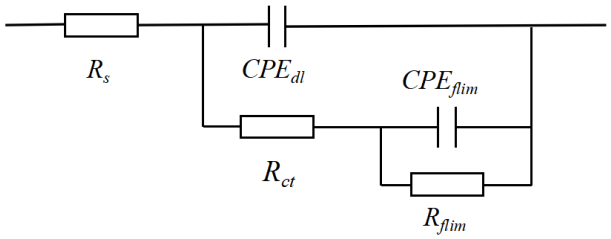

Figure 7. The equivalent electrical circuit for the EIS

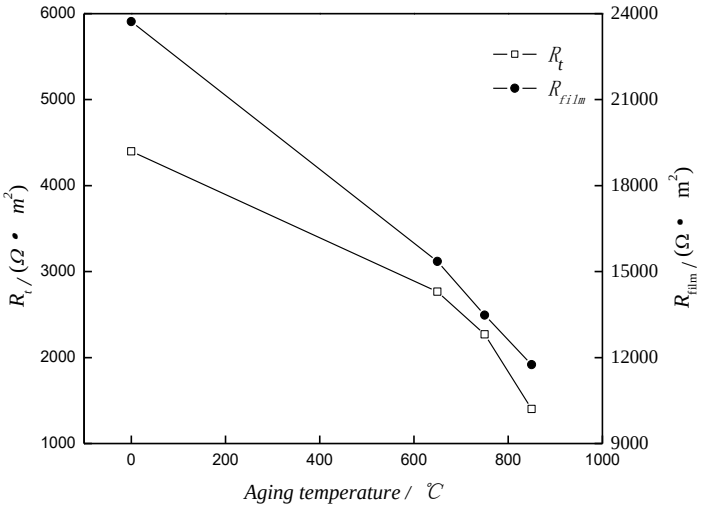

Figure 8. Effect of aging temperature on charge transfer resistance R_{ct} and R_{film} of S32750 SDSS

3.5 Effect of aging temperature on Mott-Schottky curves

From the above discussion, it could be concluded that a complete passive film may be formed on S32750 SDSS in NaCl solution. The semiconductor properties of the passive film affected the corrosion resistance [20], and the semiconductor behavior may be analyzed by Mott-Schokkty curves, and the relationship between capacitance and applied potential was calculated by the following equations [21-22]:

$$\text{for n-type semiconductor: } \frac{1}{C^2} = \frac{2}{\varepsilon\varepsilon_0 e N_D}\left(E - E_{fb} - \frac{KT}{e}\right) \quad (1)$$

$$\text{for p-type semiconductor: } \frac{1}{C^2} = -\frac{2}{\varepsilon\varepsilon_0 e N_A}\left(E - E_{fb} - \frac{KT}{e}\right) \quad (2)$$

where C is the space charge layer capacitance, ε is the dielectric constant of the film (15.6), ε_0 is the dielectric constant of the oxide film (8.854×10^{-14} F·cm^{-1}), and e is the electronic charge (1.602×10^{-19} C). The carrier concentration of the passive film formed on the S32750 SDSS can be defined as the donor densities (N_D) and the acceptor densities (N_A). E is the applied potential, E_{fb} is the flat band potential, K is the Boltzmann constant (1.38×10^{-23} J·K^{-1}), and T is the thermodynamic temperature. N_D and N_A could be estimated from the slope of the straight lines in different zones of C^{-2}~E plots.

The Mott-Schottky plots of S32750 SDSS at different aging temperatures are illustrated in Figure 9. The previous studies have proved that the passive films on the surface of stainless steel consisted of iron oxides and chromium oxides. When the potential was lower than 0.3 V, the slope of the curves were

positive, displaying that the passive film appeared as an n-type semiconductor. When the potential continued to increase, the slope of the Mott-Schokkty curves changed from positive to negative, and the passive film displayed a p-type semiconductor [23].

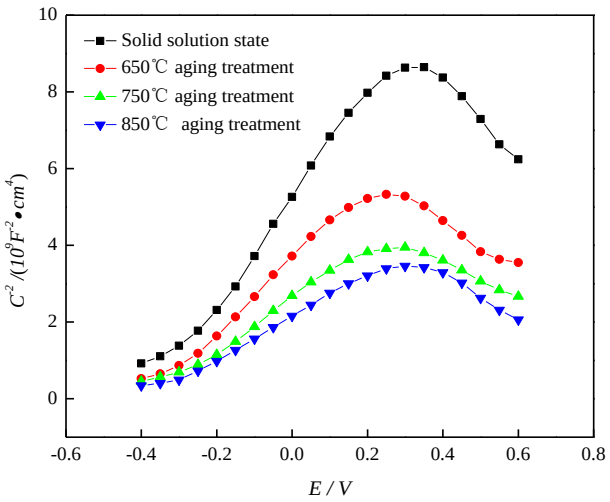

Figure 9. Mott-Schottky plots of S32750 SDSS with different aging temperature in simulated seawater

Table 4 shows the calculated results of N_A and N_D. It could be seen that the N_A and N_D values were the lowest for the S32750 SDSS sample under solid solution condition. As the aging temperature increased, the slopes of the Mott-Schottky curves decreased, and the N_A and N_D of the passive films increased gradually, which could be attributed to the σ precipitated phase resulted in the heterogeneity of the chemical composition in the duplex stainless steel [24].

Table 4. N_D and N_A of S32750 SDSS with different aging temperature in simulated seawater

Aging Temperatures	N_A(cm^{-3})	N_D(cm^{-3})
solid solution condition	8.57×10^{20}	7.84×10^{20}
650℃	1.42×10^{21}	1.27×10^{21}
750℃	1.98×10^{21}	1.83×10^{21}
850℃	2.22×10^{21}	2.35×10^{21}

As it is well established, the Cr and Mo are the main elements that give stainless steel an excellent corrosion resistance. Cr may form a stable and dense Cr_2O_3 oxide film on the surface of the stainless steel, and Mo not only participates in the formation of passive film, but also could repair quickly the passive film once it was broken, thus, the Mo improves the self-repairing ability of the passive film. The precipitation of σ phase leaded to uneven distribution of Cr and Mo in the passive film, and affected the uniformity, continuity and compactness of the passive film on the surface of the samples, therefore, the stability and corrosion resistance of the passive film were weakened. From above analysis on

microstructure image and precipitates, it could be found that the σ phase was not precipitated in the sample under the solid solution condition and aging temperatures 650 ℃. At this time, Cr and Mo may still be evenly distributed, and the performance of the passive film on the stainless steel surface was not significantly affected. When the aging temperature moved to 750 ℃, the σ phase began to precipitate, and the distribution of Cr and Mo manifested an uneven trend. The number of σ phase at 850 ℃ was further increased, and the contents of Cr and Mo at the grain boundaries of ferrite and austenite were reduced drastically, and both elements were no longer uniformly distributed in the structure. On the one hand, a large number of corrosion micro-batteries were formed [25] because of the inhomogeneous passive film. On the other hand, the uneven distribution of Cr and Mo also increased the weak positions of the passive film attacked by Cl^-, which leaded to an increase in the dissolution rate of passive film and an increasing corrosion rate.

The thickness of the passive film on the surface of the material was approximately proportional to the thickness L_{ss} of the space charge layer. The L_{ss} is calculated as follows [26]:

$$L_{ss} = \frac{\varepsilon\varepsilon_0 A}{C} \tag{3}$$

Where A is the passive film area (cm^2).

Figure 10 is a graph obtained by calculating the passive film thickness based on the Mott-Schottky measurement results, it could be seen that the thickness of the passive film decreased, implying that the stability of the passive film gradually decreased with the increase of the aging temperature, and the corrosion tendency of S32750 SDSS increased with the decreasing thickness of passive films, and it was obvious that the continuous thinning of passive film reduced the resistance for corrosion.

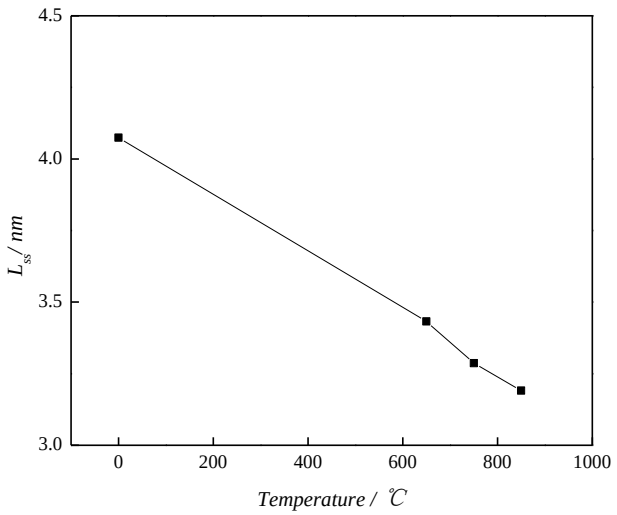

Figure 10. Passive film thickness L_{ss} of S32750 SDSS at different aging temperatures

4. CONCLUSIONS

(1) Under solid solution condition and aging temperature 650 ℃, no σ precipitation phase was found in S32750 SDSS. From 750 ℃ to 850 ℃, σ phase precipitation increased gradually. The presence of σ precipitated phase leaded to increasing inhomogeneity, defects number, and decreasing thickness of the passive films on the surface of S32750 SDSS, which eventually resulted in an weakened the

corrosion resistance of the material in simulated seawater at 5 ℃.

(2) S32750 SDSS exhibited a lower pitting potential and self-corrosion potential, higher Tafel slopes (β_a) and passivity current density with increasing aging temperature from 650 ℃to 850℃, and the R_{ct} and R_{flim} also decreased with aging temperature, which was indicated that aging treatment reduced the corrosion resistance of the material.

ACKNOWLEDGEMENTS
The present research is financially supported by Natural Science Foundation of Department of Science ＆Technology of Liaoning Province (*No*. 20180550348).

References

1. M.C. Theodoro, V.F. Pereira, P.R. Mei, A.J. Ramirez, *Metall. Mater. Trans. B,* 46(2015)1440
2. M. Shamanian, M. Mohammadnezhad, M. Amini, A. Zabolian, J.A. Szpunar, *J. Mater. Eng. Perform.,* 24(2015)3118
3. M. Campos, A. Bautista, D. Cáceres, J. Abenojar, J.M. Torralba, *J. Eur. Ceram. Soc.,* 23(2003)2813
4. M. Liljas, P. Johansson, H.P. Liu, C.O.A. Olsson, *Steel. Res. Int.,* 79(2008)466
5. D. Zou, Y. Han, W. Zhang, J. Yu, *J. Wuhan. Univ. Technol.,* 26(2011)183
6. A. Bhattacharya, P.M. Singh, *Metall. Mater. Trans. A,* 40(2009)1388
7. W. Vélez, F. Matta, P. Ziehl, *Mater. Struct.,* 49(2016)507
8. W. Wu, W.K. Hao, Z.Y. Liu, X.G. Li, C.W. Du, W.J. Liao, *J. Mater. Eng. Perform.,* 24(2015)4636
9. D.Z. Zhang, X.H. Gao, G.Q. Su, L.X. Du, Z.G. Liu, J. Hu, *J. Mater. Eng. Perform.,* 26(2017)2599
10. Y.A. Villagrán Zaccardi, A. Bértora, A.A. Di Maio, *Mater, Struct.,* 46(2013)1527
11. Y.E. Guo, P. Liang, Y.H. Shi, Y. Zhao, F. Li, L. Jin, *Int. J. Electrochem. Sci.,* 13(2018)10302
12. I. Mészáros, J. Prohászka, *J. Mater. Process. Tech.,* 161(2005)162
13. T. Berecz, É. Fazakas, I. Mészáros, I. Sajó, *J. Mater. Eng. Perform*., 24(2015)4777
14. N. Palsson, R. Pettersson, S. Wessman, J.S. Pan, *Corros. Sci*., 52(2010)179
15. H.X. Wan, C.W. Du, Z.Y. Liu, D.D. Song, X.G. Li, *Ocean. Eng.,* 114(2016)216
16. X.Q. Cheng, X.G. Li, C.W. Du, *Chinese. Sci. Bull.,* 54(2009)2239
17. M.G.S. Ferreira, N.E. Hakiki, G. Goodlet, S. Faty, A.M.P. Simões, M.D.C. Belo, *Electrochim. Acta,* 46(2001)3767
18. W. Gathright, M. Jensen, D. Lewis, *J. Mater. Sci.,* 47(2012)1677
19. P. Vijay, A. Upadhyaya, *T. Indian. I. Metals,* 61(2008)255
20. C.A. Gervasi, M.E. Folquer, A.E. Vallejo, P.E. Alvarez, *Electrochim. Acta,* 50(2005)1113
21. F.R. Attarzadeh, N. Attarzadeh, S. Vafaeian, A. Fattah-Alhosseini, *J. Mater. Eng. Perform.,* 25(2016) 4199
22. A. Fattah-Alhosseini, O. Imantalab, F.R. Attarzadeh, *J. Mater. Eng. Perform.,* 25(2016)4478
23. Z.C. Feng, X.Q. Cheng, C.F. Dong, L. Xu, X.G. Li, *Corros. Sci.,* 52(2010)3646
24. W.S. Li, J.L. Luo, *Electrochem. Commun.,* 1(1999)349
25. Y.F. Cheng, J.L. Luo, *Appl. Surf. Sci.,*167(2000)113
26. M. BenSalah, R. Sabot, E. Triki, L. Dhouibi, Ph. Refait, M. Jeannin, *Corros. Sci.,* 86(2014)61